AGILE: GIScience Series, 7, 34, 2026. https://doi.org/10.5194/agile-giss-7-34-2026
Proceedings of the 29th AGILE Conference on Geographic Information Science, 16–19 June 2026.
Eds.: Evelyn Uuemaa, Alexander Kmoch, Holger Virro, and Simon Scheider
This contribution underwent peer review based on a full paper submission.

Beyond distance: assessing heat vulnerability through mobility-based accessibility to cooling resources

Muchun Li [1], Alexis Comber [1], and Arjan Gosal [1]

[1] School of Geography, University of Leeds, Leeds, UK

Correspondence: Muchun Li (pdxm8161@leeds.ac.uk)

Abstract. Extreme heat has increasingly threatened urban health and well-being, making the assessment of heat vulnerability a growing research priority. Existing heat vulnerability studies mainly focus on coarse administrative or census-level scales and define adaptive capacity as distance-based accessibility of cooling resources. As a result, fine-scale spatial heterogeneity in heat vulnerability and the thermal burden experienced during travel to inform heat adaptation strategies are often overlooked. Considering these limitations, this study proposed a novel heat vulnerability framework that incorporates heat exposure based on a modified temperature-humidity index (MTHI), grid-level sensitivity and mobility-based adaptive capacity in relation to accumulated heat stress. A case study of Wuhan showed distinct urban-rural differences, with urban vulnerability driven by high exposure and sensitivity, and rural vulnerability shaped by limited accessibility to cooling resources. This research emphasises the importance of incorporating fine-scaled measures of mobility and heat stress into heat vulnerability assessments to better support targeted planning and heat mitigation strategies.

Submission Type. model, analysis, case study

BoK Concepts. [AM11] Network analysis, [GC2] Spatial simulation modelling,

Keywords. Heat vulnerability, Heat stress accumulation, Mobility-based accessibility

1 Introduction

Global warming has become the most critical environmental issue in recent decades, threatening human society and ecosystems worldwide (Cramer et al., 2018). The increasing frequency and severity of hot days dramatically influence human well-being, leading to increased attention on heat vulnerability. The framework proposed by the Intergovernmental Panel on Climate Change (IPCC) in its Fourth Assessment Report (AR4) (IPCC, 2007) describes a heat vulnerability index (HVI), shaped by exposure, sensitivity, and adaptive capacity, which has been developed and widely applied (Estoque et al., 2023).

Exposure was defined as 'the nature and degree to which a system is exposed to significant climate variations' (IPCC, 2007). To characterise exposure, satellite-derived land surface temperature (LST) has been widely utilised due to its high spatial resolution (Sun et al., 2022). Other meteorological factors, such as humidity and wind speed, can also affect subjective sensations and health consequences of urban residents (Yin et al., 2019; Zhang et al., 2023). Heat stress indices, such as the wet bulb-globe temperature index (WBGT) and the universal thermal climate index (UTCI), provide detailed information on exposure but rely on on-site observations with limited spatiotemporal resolution (Cheng et al., 2021; Ho et al., 2025).

Adaptive capacity was defined as 'the ability of a system to adjust to climate change (including climate variability and extremes), to moderate potential damages, to take advantage of opportunities, or to cope with the consequences' (IPCC, 2007). To quantify adaptive capacity, existing studies have predominantly focused on distance-based access to cooling sources (Cheng et al., 2021), while the thermal burden individuals experience during travel has been largely overlooked. Basu et al. (2024) found that heat stress significantly increases perceived walking distances and reduces overall pedestrian accessibility, suggesting distance-based measures may bias assessments of effective accessibility and adaptive capacity.

Empirical studies have demonstrated that heat stress accumulates over time, significantly increasing the incidence of heat-related symptoms, including dizziness,

hyperhidrosis, chest tightness and potentially fatal heatstroke (Huang et al., 2025; Zhao et al., 2024). Thus heat stress constrains outdoor mobility by reducing activity frequency, slowing travel speeds and shortening travel distances (Creemers et al., 2015; Jia et al., 2022; Wu and Liao, 2020). As a result, cooling resources may become effectively inaccessible even when located nearby. These findings highlight the need for an approach that integrates both mobility-related heat cost and its accumulated effect into adaptive capacity assessment.

To address this gap, this study proposes a novel and comprehensive framework for evaluating heat vulnerability. Heat exposure is characterised using a modified temperature-humidity index (MTHI) derived from land surface temperature (LST) and the normalised difference moisture index (NDMI). Heat stress is defined using an MTHI-based grading scheme, which clarifies that only heat exposure beyond the defined threshold heat stress starts to accumulate. Adaptive capacity is conceptualised as a function of heat stress accumulation and distance required to access cooling resources. This framework also integrates an origin-destination (OD) cost matrix constructed from road network to simulate the thermal burden experienced by residents during purposeful travel to cooling resources. Through a detailed case study, this approach enables higher-resolution mapping and a more detailed identification of spatial variations in heat vulnerability.

2 Methods

2.1 Exposure index (EI) construction

Feng et al. (2020) proposed a modified temperature-humidity index (MTHI) to quantify the spatial distribution of heat exposure. This index is calculated as:

$$\mathrm{MTHI} = 1.8\mathrm{LST} + 32 - 0.55 \cdot (1 - \mathrm{NDMI}) \cdot (1.8\mathrm{LST} - 26) \quad (1)$$

In this study, LST was collected from the thermal infrared band (ST_B10) and NDMI from the near infrared band (NIR) and short-wave infrared band (SWIR) of Landsat 8. To verify the applicability of the MTHI, Feng et al. (2023) calculated the physiological equivalent temperature (PET) using meteorological station data and found a strong statistical correlation between MTHI and PET. Their findings indicated that MTHI is reliable for characterising the exposure index (EI). Consequently, a growing body of research has utilised MTHI to characterise thermal comfort across both urban and rural contexts, while exploring its associations with land cover change and electricity consumption (Hidalgo-García et al., 2025; Hu et al., 2024; Nguyen et al., 2024).

To characterise heat stress for adaptive capacity assessment, this study adopts an MTHI grading scheme (Qi et al., 2022; Yang et al., 2025). The grading principle of using the mean-standard deviation method for thermal comfort classification is shown in Tab. 1, where μ and σ are the mean and the standard deviation of MTHI, respectively. The normality of the MTHI distribution was confirmed by skewness (−0.17) and kurtosis (1.09) statistics, satisfying the practical normality criteria of |skewness| < 3 and |kurtosis| < 7 (Kline, 2011). Heat stress intensity is defined as values exceeding the threshold of $\mu + 0.5\sigma$, including categories classified as "Discomfortable" and "More Discomfortable".

Table 1. Thermal comfort (MTHI) grading.

Range of value	Meaning
$\mathrm{MTHI} \leq \mu - \sigma$	More comfortable
$\mu - \sigma < \mathrm{MTHI} \leq \mu - 0.5\sigma$	Comfortable
$\mu - 0.5\sigma < \mathrm{MTHI} \leq \mu + 0.5\sigma$	Less comfortable
$\mu + 0.5\sigma < \mathrm{MTHI} \leq \mu + \sigma$	Discomfortable
$\mu + \sigma < \mathrm{MTHI}$	More discomfortable

2.2 Sensitivity index (SI) construction

Sensitivity captures population socio-demographic characteristics (Cheng et al., 2021; Kumar and Sharma, 2020). Owing to the poor thermoregulation ability of the elderly and children, age has been recognised as one of the crucial sensitivity factors (Grubenhoff et al., 2007; Hansen et al., 2011). Previous studies found that heat-related mortality is higher among people with less education, poorer living conditions and social isolation (Mallen et al., 2019; Schwarz et al., 2025). Similar results were also found in outdoor workers, emphasising the need for adding relevant variables into sensitivity assessment (Venugopal et al., 2021). While indicators such as education level, living alone, and housing conditions are categorised as adaptive capacity in some studies, here they were classified as sensitivity, emphasising their role as pre-existing, relatively fixed household attributes.

In this study, 8 block-level variables from census data were used based on literature reviews and local conditions of the study area. These variables were spatially interpolated to a grid-level population dataset (Comber and Zeng, 2019) (Tab. 2). Collinearity among variables may affect the construction of the sensitivity index (SI), highlighting the need for principal component analysis (PCA) (Fang and Zhao, 2024). To ensure cross-indicator comparability, the z-score method was applied to standardise all variables to a uniform scale, with a mean of 0 and a standard deviation of 1. In detail, PCA was performed to extract m principal components with eigenvalues λ_j $(j = 1, \cdots, m)$ .The weight of the i_{th} indicator was calculated as follows:

$$w_i = \sum_{j=1}^{m} \frac{\lambda_j}{\sum_{j=1}^{m} \lambda_j} \cdot l_{ij}^2 \quad (2)$$

where l_{ij}^2 is the factor loading of indicator i on the j_{th} principal component, λ_j is the eigenvalue of the j_{th} principal component, and m is the number of retained components. Finally, SI for each grid was calculated as follows:

$$SI = \sum_{i=1}^{n} w_i \cdot Z_i \quad (3)$$

where Z_i is the standardised value of the indicator i. w_i is the weight of each indicator. In this study, the KMO value of 0.831, together with a significant Bartlett's test ($p < 0.01$), indicates that the selected variables are appropriate for PCA. Through this process, a grid-level sensitivity map was generated.

Table 2. Sensitivity variables description.

Indicators	Description
Age rate ≥ 65	Population aged over 65 years
Age rate ≤14	Population aged below 14 years
Agriculture/forestry/fishery population	Population engaged in agriculture/forestry/fishery
Construction population	Population engaged in construction activities
Elderly living alone	Population living alone aged over 65
Living without elevator	Population living without an elevator
Illiteracy rate	Population illiterate aged over 15 years
Below associate degree	Population without associate or higher degree

2.3 Adaptive capacity index (ACI) construction

In this study, adaptive capacity reflects contextual influences which influence residents' ability to access cooling resources. To define adaptive capacity, heat stress accumulation (HSA) was calculated based on travel distance and heat stress. While exposure characterises the baseline thermal environment of residents' normal living context, HSA captures the potential heat cost incurred during purposeful travel to cooling resources.

The calculation of the ACI proceeded as follows: First, an OD cost matrix was initialised using road network, with population grids as origins and cooling resources as destinations. The population grids were derived from a population raster, which included only cells with values greater than zero, whereas cooling resources comprise green spaces, blue spaces, and medical facilities. Second, MTHI values were processed in ArcGIS to retain only differences relative to the threshold defined by the grading scheme (Tab. 1), with values below the threshold set to zero. Third, HSA during travel was incorporated as the cost constraint. For each road segment, processed MTHI values were directly extracted at points along road segments, and the mean of these values was multiplied by the segment length. The heat cost for segment s was calculated as follows:

$$C_S = \overline{HS_s} \cdot L_s \quad (4)$$

where C_S denotes the heat cost of road segment s, HS_s represents the mean heat stress along the segment s, and L_s is its length. Based on this definition, the HSA along a path p, connecting a population grid i to a cooling facility j, was calculated as the sum of heat costs across all segments composing the path:

$$HSA_{p(i,j)} = \sum_{s \in p(i,j)} C_s \quad (5)$$

For each population grid cell, the minimum HSA was identified as the lowest thermal burden to access any cooling resource. Finally, an adaptive capacity index (ACI) was then constructed by integrating the minimum HSA across all cooling resources. Specifically, ACI was calculated as follows:

$$ACI_C = \beta \cdot \min(HSA_{c,k}) + (1 - \beta) \cdot \overline{HSA_{c,k}} \quad (6)$$

where $HSA_{c,k}$ denotes the HSA of grid cell C with respect to resource type k, $\min(HSA_{c,k})$represents the minimum heat cost across all cooling resource types, and $\overline{HSA_{c,k}}$ is the mean accessibility across all types. The balancing coefficient β ($0 \leq \beta \leq 1$) was set to 0.5 to reflect a balanced prioritisation between the minimum and mean heat cost components, consistent with a general-population vulnerability scenario. A higher ACI indicates greater difficulty accessing cooling resources, reflecting lower adaptive capacity and thus higher overall heat vulnerability.

2.4 HVI construction

In this study, composite HVI was constructed using multiplicative aggregation to reflect interdependent effects among components. Prior to multiplication, the value of EI, SI, and ACI were normalised using Min-Max scaling as follows:

$$x' = 0.1 + \frac{x - MIN}{MAX - MIN} \cdot 0.9 \quad (7)$$

Finally, HVI was calculated as follows:

$$HVI = EI \cdot SI \cdot ACI \quad (8)$$

2.5 Data and software availability

This study uses publicly available remote sensing, geospatial, and census datasets (Tab. 3). Landsat 8 satellite imagery was collected from USGS EarthExplorer (https://earthexplorer.usgs.gov). The road network in Wuhan was collected from OpenStreetMap

(https://www.openstreetmap.org). Cooling resource data, including green and blue spaces, were derived from Landsat 8 imagery using the Normalised Difference Vegetation Index (NDVI) and Modified Normalised Difference Water Index (MNDWI). Pixels with NDVI > 0.3 were classified as vegetation, and pixels with MNDWI > 0 were classified as water bodies, following standard thresholds for urban green and water features (Qi et al., 2025), as shown in Fig. 1(a). These processing steps were implemented using ArcGIS software. Cooling resources relevant to medical services were obtained via the Amap (https://www.amap.com/), as shown in Fig. 1(b). Sensitivity-related variables were collected from the Seventh Population Census in Wuhan and downloaded from the local chronicles office (http://dfz.wuhan.gov.cn/). The population dataset was derived from the Age-Stratified Population Estimation from the 2020 China Census by Township (ASPECT) (Ju et al., 2025). The Python code for generating the proposed HVI framework is available on GitHub (https://github.com/AGILE/heat-vulnerability-framework).

Table 3. Data sources and types.

Data	Type
Landsat 8 satellite imagery	30 m raster
Seventh National Population (2020 Census)	Vector polygon
Age-Stratified Population Estimation (2020 Census)	100 m raster
Medical services POI (Amap)	Vector point
Road network data (OpenStreetMap)	Vector line

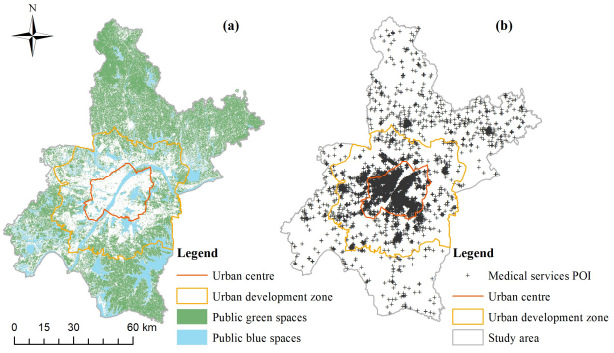

Figure 1. Spatial patterns of public green and blue spaces (a) and medical services POI (b) with geographical location of urban centre and urban development zone in Wuhan.

4 Results

4.1 Spatial distribution of EI

As shown in Fig. 2(a), overall heat exposure levels are higher in western regions and lower in eastern regions, reflecting a pronounced spatial gradient across Wuhan.

For adaptive capacity analysis, heat stress was characterised using the MTHI grading in Table 1. Areas classified as the most discomforting areas ($\mu + \sigma <$ MTHI) are primarily located in the southwestern region (Fig. 2(b)). Regions under relatively comfort (MTHI $\leq \mu + 0.5\sigma$) are primarily distributed near urban blue and green spaces, particularly in central and eastern Wuhan. In these locations, blue spaces and their surrounding green spaces work together to mitigate heat stress within the urban environment.

To better understand the drivers of this spatial pattern, the spatial distributions of LST and NDMI were further analysed. Fig. 2(c) shows the spatial distribution of LST, which exhibits a pronounced contrast between urban and rural areas, reflecting the urban heat island effect. LST in urban centres can reach 70 °C. In contrast, NDMI, which reflects vegetation water content and correlates with relative humidity, exhibits an opposite spatial trend as shown in Fig. 2(d). This may be due to vegetation being sparse in urban centres, with high land-use competition, whereas the surrounding urban areas feature more abundant greenery, including green wedges, parks, and ecological buffer zones. At the peripheral margins of urban development zones, blue-green spaces with increased density engender heightened humidity, leading to an increase in the MTHI and thereby compounding thermal discomfort among the exposed population.

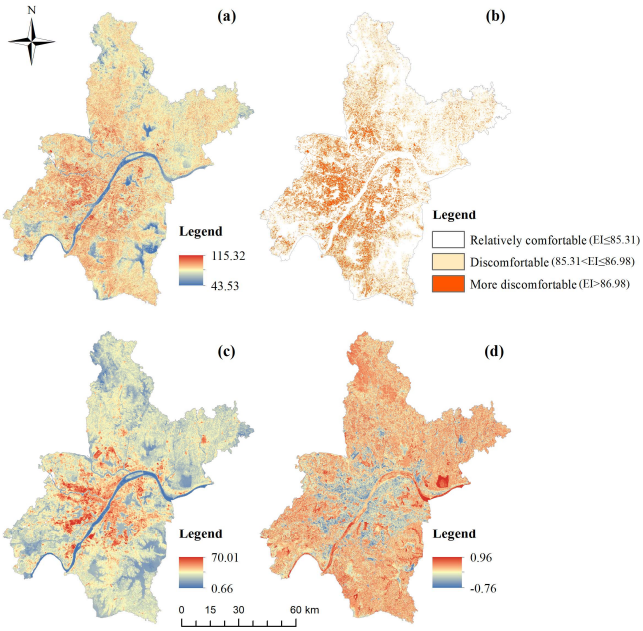

Figure 2. Spatial patterns of MTHI (a), grading results of MTHI (b), LST (c), and NDMI (d) in Wuhan.

4.2 Spatial distribution of SI

As shown in Tab. 4, two principal components were retained to construct the composite SI, which together explain 89.7% of the variation in the block-level census data. All variables from Tab. 2 contribute to the final SI

through weights derived from their factor loadings across both components. As for the contribution of each variable, education level, lack of elevators, and age structure, including the population aged over 65 and under 14, all demonstrate relatively high contribution, with all weights exceeding 0.7. Among them, education level made the greatest contribution, with a weight of 0.81. Elderly people living alone and illiteracy also show notable influence, with weights of 0.686 and 0.651, respectively. By comparison, occupational indicators are of limited importance, particularly the proportion of the population engaged in agriculture, forestry, and fisheries, which has a weight of 0.171.

Table 4. Principal components extracted to build sensitivity index (SI).

Principal Components	Extraction Sums of Squared Loadings		
	Total (eigenvalue)	% of Variance	Cumulative %
PC_1	5.961	74.508	74.508
PC_2	1.216	15.202	89.710

As shown in Fig. 3, SI values exhibit a clear spatial clustering pattern. High-sensitivity areas are primarily concentrated in the urban centre. Several secondary hotspots are also observed in suburban built-up areas. This pattern may partly be attributable to population density. As a result, rural areas are mostly characterised by very low SI values due to their lower population density. Overall, the spatial pattern of SI suggests an urban-rural gradient, with the sensitive population concentrated in the urban centre with high heat exposure.

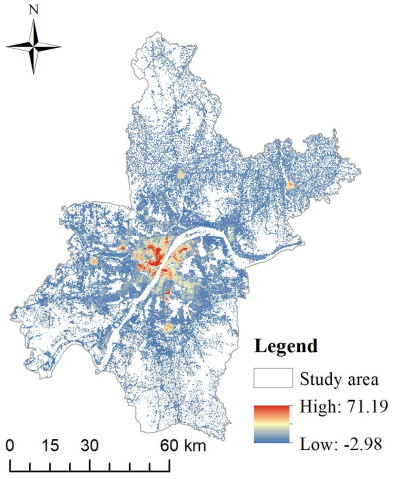

Figure 3. Spatial patterns of SI in Wuhan.

4.3 Spatial distribution of ACI

In this study, ACI was calculated as a function of travel distance and average heat stress. As shown in Fig. 4, the average heat stress was calculated for each road segment. Each road segment was classified into one of five categories using the natural breaks method, with values ranging from 0 to 12.66. Overall, higher values are concentrated in urban development zone, particularly in the southwestern part of the study area, whereas lower values are observed mainly in rural areas. These areas are largely classified as relatively comfortable according to the MTHI grading. As expected, average heat stress exhibits a clear decreasing trend from the urban centre towards the urban periphery.

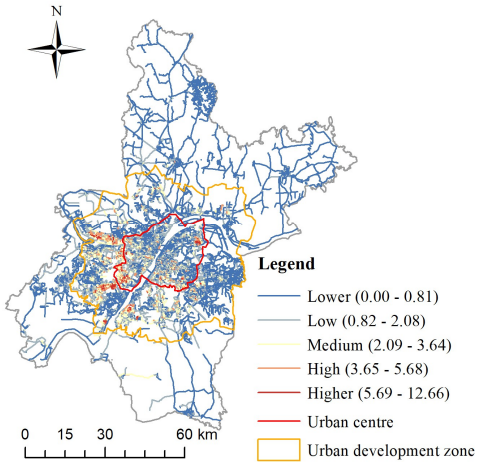

Figure 4. Spatial patterns of classified average heat stress in Wuhan.

Fig. 5(a) illustrates the spatial distribution of ACI from the proposed heat-stress-integrated method, expressed as the accumulated heat stress. In contrast to the pattern observed in Fig. 4, most high values are in rural areas. These areas are typically situated on the urban periphery and are distant from major road networks, which substantially increases the cost of accessing cooling resources, even though they live in relatively comfortable thermal conditions. By contrast, urban areas exhibit very low heat costs due to both higher road network density and the widespread availability of cooling resources, especially medical facilities. The spatial pattern of ACI exhibits a clear core-periphery gradient, with heat costs remaining low in the urban centre and increasing progressively towards suburban and rural areas.

Fig. 5(b) presents the spatial distribution of ACI derived from the traditional distance-based method, which considers only travel distance to cooling resources. Compared to Fig. 5(b), the reduction in ACI in rural areas under the heat-stress-integrated method is primarily attributable to the more comfortable thermal background compared to urban areas, which lowers the heat cost of travel to cooling resources. Areas exhibiting the most pronounced ACI increases are concentrated at the boundaries of the urban centre and in areas between urban centre and urban development zone. Although these areas contain more green-blue spaces than the urban core, the

high density of construction and industrial activities generates intense heat stress, increasing the heat cost for residents accessing nearby cooling facilities. Conversely, despite the relative scarcity of green-blue spaces in the urban centre, ACI values are lower under the proposed method than under the distance-based approach. This suggests that the relatively mild thermal environment, although still mainly classified as discomfortable areas, partially compensates for limited cooling resources, details that distance-based measures are unable to capture.

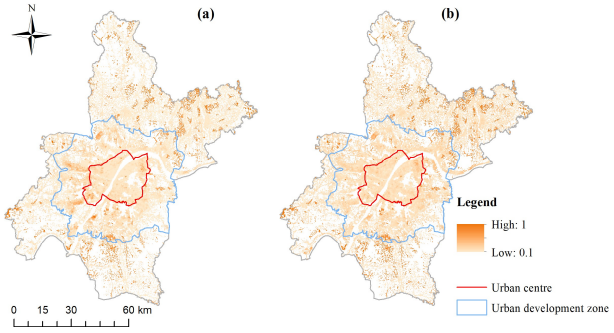

Figure 5. Spatial patterns of ACI derived from heat-stress-integrated method (a) and distance-based method (b).

4.4 Spatial distribution of HVI

Fig. 6 illustrates the spatial distribution of the composite HVI across the study area. As shown in Fig. 6(a), the HVI ranges from 0.003 to 0.139, indicating pronounced heterogeneity across the study area. Overall, high HVI areas are mainly located in urban centre or rural areas far from the road network. High heat vulnerability in urban centres is driven by high exposure and sensitivity. However, the intensity of exposure and vulnerability associated with population concentration and land-use competition tends to diminish towards the urban periphery as population density decreases. Vulnerability is particularly low in areas surrounding urban blue and green spaces. In contrast, high heat vulnerability in remote rural areas is primarily influenced by adaptive capacity. Although these areas are often located near green spaces, access to additional cooling resources, such as medical facilities and blue areas, requires considerable travel distance and heat costs, thereby reducing overall adaptation. Furthermore, uneven road network density exacerbates inequalities in resource accessibility, ultimately increasing heat vulnerability.

Fig. 6(b) presents the spatial difference in HVI between the proposed framework with heat stress accumulation and the traditional framework focused on distance-based accessibility. In the urban centre, HVI values decrease under the proposed method, as the relatively moderate thermal environment along urban travel routes reduces the heat cost of accessing cooling resources (Fig. 6(d)). In contrast, HVI values increase markedly in areas between the urban centre and the urban development zone, where intense human activities elevate local heat stress and substantially raise the heat cost of travel (Fig. 6(c)). In rural areas, HVI values decrease under the proposed method, as the relatively comfortable thermal environment partially offsets the disadvantage of greater travel distances (Fig. 6(e)). These patterns collectively demonstrate that distance-based measures systematically misrepresent overall vulnerability across both urban and rural contexts.

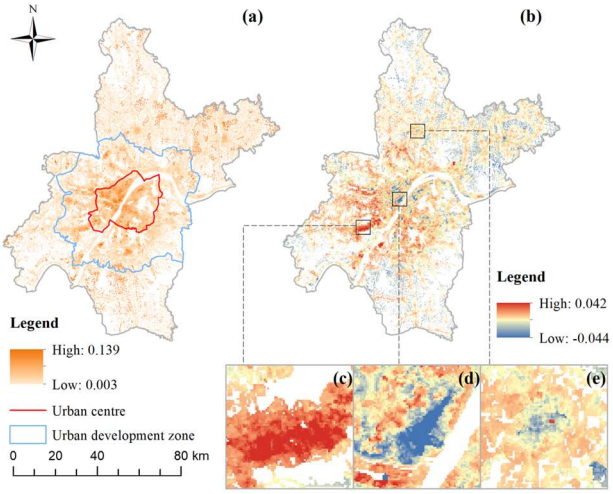

Figure 6. Spatial patterns of HVI from the proposed method (a), HVI difference between the proposed and traditional methods (b), and Zoomed-in views of selected sub-regions (c~e).

5 Discussion and Conclusions

The main objective of this study is to characterise heat vulnerability in detail by introducing a novel analytical framework and considering the influence of heat cost on adaptive capacity assessment in heat vulnerability research. To this end, detailed heat exposure information was first derived by calculating the MTHI index based on temperature and humidity. An OD cost matrix was then constructed to simulate the accumulated heat stress experienced by residents during purposeful travel to cooling resources. Specifically, this study calculated both the average heat stress along travel routes and heat stress accumulation associated with travel distance. The results provide greater spatial detail than conventional census-based and distance-based vulnerability studies, offering more informative evidence for local policy making and urban planning.

The use of MTHI for exposure assessment is a necessary simplification given the research aims. However, residents' daily mobility, including commuting and other routine activities, may alter their actual heat exposure (Zhang et al., 2026). Empirical research has shown that both willingness to move and speed may change with the accumulation of heat stress, potentially influencing route

choice and destination selection (Basu et al., 2024). These dynamic behavioural responses were not incorporated in the present analysis, as this study focuses on exploring heat vulnerability under a generalised scenario. Future research could integrate high-resolution mobility data, such as mobile or social media data, to better capture actual daily mobility patterns.

Regarding cooling resources selection, this study considered green-blue spaces and medical facilities; however, indoor air-conditioned environments such as shopping centres should also be incorporated. Previous studies also found a threshold effect between the size of green-blue spaces and their cooling efficiency (Yu et al., 2020). Compared to the present study, which relied solely on NDVI and MNDWI thresholds to identify cooling destinations, future research should adopt a multi-criteria approach to more comprehensively define cooling resources that truly contribute to heat adaptation.

In this study, only cumulative heat stress associated with walking was considered. The influence of other travel modes on adaptive capacity warrants further investigation. Finally, validation of the proposed framework and its application across diverse geographical contexts remains an important direction for future research.

Declaration of Generative AI in writing

The authors declare that they have not used Generative AI tools in the preparation of this manuscript. All intellectual and creative work, including the analysis and interpretation of data, is original and has been conducted by the authors without AI assistance.

References

Basu, R., Colaninno, N., Alhassan, A., and Sevtsuk, A.: Hot and bothered: Exploring the effect of heat on pedestrian route choice behavior and accessibility, Cities, 155, 105435, https://doi.org/10.1016/j.cities.2024.105435, 2024.

Cheng, W., Li, D., Liu, Z., and Brown, R. D.: Approaches for identifying heat-vulnerable populations and locations: A systematic review, Sci. Total Environ., 799, 149417, https://doi.org/10.1016/j.scitotenv.2021.149417, 2021.

Comber, A. and Zeng, W.: Spatial interpolation using areal features: A review of methods and opportunities using new forms of data with coded illustrations, Geogr. Compass, 13, e12465, https://doi.org/10.1111/gec3.12465, 2019.

Cramer, W., Guiot, J., Fader, M., Garrabou, J., Gattuso, J.-P., Iglesias, A., Lange, M. A., Lionello, P., Llasat, M. C., Paz, S., Peñuelas, J., Snoussi, M., Toreti, A., Tsimplis, M. N., and Xoplaki, E.: Climate change and interconnected risks to sustainable development in the Mediterranean, Nat. Clim. Change, 8, 972–980, https://doi.org/10.1038/s41558-018-0299-2, 2018.

Creemers, L., Wets, G., and Cools, M.: Meteorological variation in daily travel behaviour: evidence from revealed preference data from the Netherlands, Theor. Appl. Climatol., 120, 183–194, https://doi.org/10.1007/s00704-014-1169-0, 2015.

Estoque, R. C., Ishtiaque, A., Parajuli, J., Athukorala, D., Rabby, Y. W., and Ooba, M.: Has the IPCC's revised vulnerability concept been well adopted?, Ambio, 52, 376–389, https://doi.org/10.1007/s13280-022-01806-z, 2023.

Fang, Y. and Zhao, L.: Exploring the supply-demand match and drivers of blue-green spaces cooling in Wuhan Metropolis, URBAN Clim., 58, 102194, https://doi.org/10.1016/j.uclim.2024.102194, 2024.

Feng, L., Zhao, M., Zhou, Y., Zhu, L., and Tian, H.: The seasonal and annual impacts of landscape patterns on the urban thermal comfort using Landsat, Ecol. Indic., 110, 105798, https://doi.org/10.1016/j.ecolind.2019.105798, 2020.

Feng, R., Wang, F., Liu, S., Qi, W., Zhao, Y., and Wang, Y.: How urban ecological land affects resident heat exposure: Evidence from the mega-urban agglomeration in China, Landsc. Urban Plan., 231, 104643, https://doi.org/10.1016/j.landurbplan.2022.104643, 2023.

Grubenhoff, J. A., Du Ford, K., and Roosevelt, G. E.: Heat-Related Illness, Clin. Pediatr. Emerg. Med., 8, 59–64, https://doi.org/10.1016/j.cpem.2007.02.006, 2007.

Hansen, A., Bi, P., Nitschke, M., Pisaniello, D., Newbury, J., and Kitson, A.: Perceptions of Heat-Susceptibility in Older Persons: Barriers to Adaptation, Int. J. Environ. Res. Public. Health, 8, 4714–4728, https://doi.org/10.3390/ijerph8124714, 2011.

Hidalgo-García, D., Founda, D., Rezapouraghdam, H., Jiménez, A. E., and Azinuddin, M.: Urban Forest Microclimates and Their Response to Heat Waves—A Case Study for London, Forests, 16, https://doi.org/10.3390/f16050790, 2025.

Ho, H. C., Tong, S., Zhou, Y., Hu, K., Yang, X., and Yang, Y.: Mapping Heat Vulnerability and Heat Risk for Neighborhood Health Risk Management in Urban Environment? Challenges and Opportunities, Curr.

Environ. Health Rep., 12, 14, https://doi.org/10.1007/s40572-025-00478-7, 2025.

Hu, C., Zhang, M., Huang, G., Li, Z., Sun, Y., and Zhao, J.: Tracking the impact of the land cover change on the spatial-temporal distribution of the thermal comfort: Insights from the Qinhuai River Basin, China, Sustain. Cities Soc., 116, 105916, https://doi.org/10.1016/j.scs.2024.105916, 2024.

Huang, B., Matzarakis, A., and He, B.-J.: Nonlinear law of cumulative heat exposure and dynamic thermal comfort during pedestrians' walking: Field experiments and machine learning predictions, Sustain. Cities Soc., 131, 106696, https://doi.org/10.1016/j.scs.2025.106696, 2025.

IPCC: Climate Change 2001: Impacts, adaptation, and vulnerability: Working Group II Contribution to the Third Assessment Report of the Intergovernmental Panel on Climate Change, Cambridge Univ. Press, Cambridge, 1032 pp., 2001.

IPCC: Climate Change 2007: synthesis Report Contribution of Working Groups I, II and III to the Fourth Assessment Report of the Intergovernmental Panel on Climate Change (IPCC), Cambridge University Press, Cambridge, https://doi.org/10.1017/cbo9780511546013, 2007.

Jia, S., Wang, Y., Wong, N. H., Chen, W., and Ding, X.: Influences of the thermal environment on pedestrians' thermal perception and travel behavior in hot weather, Build. Environ., 226, 109687, https://doi.org/10.1016/j.buildenv.2022.109687, 2022.

Ju, Y., Liang, Y., Kong, J., Wang, X., Wen, S., Shang, H., and Wang, X.: 100-m resolution Age-Stratified Population Estimation from the 2020 China Census by Township (ASPECT), Sci. Data, 12, 1058, https://doi.org/10.1038/s41597-025-05401-1, 2025.

Kline, R. B.: Principles and Practice of Structural Equation Modeling, Guilford Press, New York, 2011.

Kumar, P. and Sharma, A.: Study on importance, procedure, and scope of outdoor thermal comfort –A review, Sustain. Cities Soc., 61, 102297, https://doi.org/10.1016/j.scs.2020.102297, 2020.

Mallen, E., Stone, B., and Lanza, K.: A methodological assessment of extreme heat mortality modeling and heat vulnerability mapping in Dallas, Texas, Urban Clim., 30, 100528, https://doi.org/10.1016/j.uclim.2019.100528, 2019.

Nguyen, C. T., Nguyen, H., and Sakti, A. D.: Seasonal characteristics of outdoor thermal comfort and residential electricity consumption: A Snapshot in Bangkok Metropolitan Area, Remote Sens. Appl. Soc. Environ., 33, 101106, https://doi.org/10.1016/j.rsase.2023.101106, 2024.

Qi, Y., Li, H., Pang, Z., Gao, W., and Liu, C.: A Case Study of the Relationship Between Vegetation Coverage and Urban Heat Island in a Coastal City by Applying Digital Twins, Front. Plant Sci., 13, https://doi.org/10.3389/fpls.2022.861768, 2022.

Qi, Y., Zhang, C., Pei, S., Yu, H., and Hu, Y.: Spatiotemporal evolution of the cooling effect of blue-green space in different LCZs: A comparative study of Wuhan and Shanghai (2000−2022), Urban Clim., 64, 102723, https://doi.org/10.1016/j.uclim.2025.102723, 2025.

Schwarz, L., Chen, C., Castillo Quiñones, J. E., Aguilar-Dodier, L. C., Hansen, K., Sanchez, J. R., González, D. J. X., McCord, G., and Benmarhnia, T.: Heat-related mortality in Mexico: A multi-scale spatial analysis of extreme heat effects and municipality-level vulnerability, Environ. Int., 195, 109231, https://doi.org/10.1016/j.envint.2024.109231, 2025.

Sun, Y., Li, Y., Ma, R., Gao, C., and Wu, Y.: Mapping urban socio-economic vulnerability related to heat risk: A grid-based assessment framework by combing the geospatial big data, Urban Clim., 43, 101169, https://doi.org/10.1016/j.uclim.2022.101169, 2022.

Venugopal, V., Shanmugam, R., and Perumal Kamalakkannan, L.: Heat-health vulnerabilities in the climate change context—comparing risk profiles between indoor and outdoor workers in developing country settings, Environ. Res. Lett., 16, 085008, https://doi.org/10.1088/1748-9326/ac1469, 2021.

Wu, J. and Liao, H.: Weather, travel mode choice, and impacts on subway ridership in Beijing, Transp. Res. Part Policy Pract., 135, 264–279, https://doi.org/10.1016/j.tra.2020.03.020, 2020.

Yang, G., Zhang, B., Zhao, Y., Wang, J., Li, Y., Gui, J., Tian, T., and Zhang, Z.: Study on the prediction model of urban surface temperature between middle and low latitudes in China, Case Stud. Therm. Eng., 72, 106333, https://doi.org/10.1016/j.csite.2025.106333, 2025.

Yin, S., Lang, W., and Xiao, Y.: The synergistic effect of street canyons and neighbourhood layout design on pedestrian-level thermal comfort in hot-humid area of China, Sustain. Cities Soc., 49, 101571, https://doi.org/10.1016/j.scs.2019.101571, 2019.

Yu, Z., Yang, G., Zuo, S., Jørgensen, G., Koga, M., and Vejre, H.: Critical review on the cooling effect of urban blue-green space: A threshold-size perspective, Urban For. Urban Green., 49, 126630, https://doi.org/10.1016/j.ufug.2020.126630, 2020.

Zhang, K., Cao, C., Chu, H., Zhao, L., Zhao, J., and Lee, X.: Increased heat risk in wet climate induced by urban humid heat, Nature, 617, 738–742, https://doi.org/10.1038/s41586-023-05911-1, 2023.

Zhang, Y., Kwan, M.-P., and Zhang, Z.: Quantifying mobility-based seasonal individual heat exposure and the NEAP using multi-source spatiotemporal data, Urban Clim., 66, 102828, https://doi.org/10.1016/j.uclim.2026.102828, 2026.

Zhao, H., Xu, G., Shi, Y., Zhai, Y., Zhao, L., and Brown, R. D.: Evaluation of pedestrian thermal comfort from a whole-trip perspective: An outdoor empirical study, Sustain. Cities Soc., 115, 105872, https://doi.org/10.1016/j.scs.2024.105872, 2024.